ISSN 1330-3651 (Print), ISSN 1848-6339 (Online) https://doi.org/10.17559/TV-20241105002110
Original scientific paper

# Enhanced Anti-Offset Method for Wireless Power Transmission using Bilateral LCC Compensation

Zhen ZHAO, ZeJun ZHAO, XinMiao TENG, DeZhou YU, Shuyao TIAN, Xu LIANG, Lian Cheng ZHANG*

**Abstract:** In this study, electric vehicle charging gun and radio energy transmission technology are integrated to overcome the problem of unstable efficiency of electric vehicle wireless power transmission (WPT) due to misalignment of the coupling coil of the charging gun. It introduces a novel dual-coupled LCC compensation circuit structure combined with a spiral-inserted magnetic core coupling coil. Using simulations in ANSYS and MATLAB, the design demonstrates stable output efficiency with deviations below 0.4% for displacements up to 30mm. This work advances WPT systems by enhancing stability and efficiency, offering a practical solution for real-world applications in electric vehicle charging.

**Keywords:** coupling coil; electric vehicle charging; LCC circuit; spiral-inserted; wireless power transmission

## 1 INTRODUCTION

In the context of the pursuit of high efficiency and energy saving in the 21st century, electric vehicles have been widely welcomed by governments and people around the world because of their higher energy efficiency ratio, lower carbon emissions and more economical and convenient use of renewable energy [1]. WPT (Wireless Power Transfer), as a new energy transmission mode, has been widely studied in the field of electric vehicles because of its safety, portability and flexibility [2]. Since WPT technology has the problem of unstable transmission efficiency, it not only increases the burden of the grid, but also may cause damage to the battery life [3]. Unstable output power will also interfere with other devices or systems connected to it, affecting the collaborative work of the entire system, so it has not been widely used.

Currently, contact charging guns [4, 5] are usually used for the power transmission of electric vehicles. If the problem of unstable transmission efficiency of Wireless Power Transfer (WPT) can be solved and WPT can be applied to the charging of electric vehicles, then power transmission without physical connection can be achieved, which can not only improve the security of power transmission but also greatly enhance its reliability, and inject strong impetus into the popularization and further development of electric vehicles. In the field of radio energy transmission, many researches focus on the problem of anti-migration, most of which are based on planar coupled coils [6]. However, as the most commonly used transmission tool for electric vehicle radio energy transmission at this stage, the working characteristics of the charging gun are not compatible with the planar coupling coil. This mismatch phenomenon makes it difficult for relevant research results to be successfully implemented in the charging gun scene, thus restricting the further popularization and expansion of radio energy transmission technology in the field of electric vehicle charging.

Therefore, in-depth exploration of the coupling coil structure compatible with the charging gun, and research on and working out effective methods to reduce the instability of transmission efficiency, is of critical significance for promoting technological innovation and industrial upgrading in related fields.

## 2 LITERATURE REVIEW

In the field of power transmission, WPT research focuses on three key aspects, namely power transmission mode, compensation circuit topology design, and coupling coil offset and its effects [7]. Next, these three research directions will be sorted out in detail, and the existing efficiency optimization situation will be discussed in depth.

### 2.1 Power Transmission Methods

WPT technology can be divided into three types according to the differences in the working principle of its power transmission mode: electromagnetic induction coupling type [8], microwave radiation coupling type [9] and magnetic resonance coupling type [10]. Among them, electromagnetic induction coupling has the advantage of lower cost [11], but the transmission distance of induction charging mode is shorter than that of resonant charging mode. And the efficiency is low [12], the transmission efficiency is usually 30%-60%. The microwave radiation type transmits high-frequency microwave in the direction of the receiving end to make the receiving end obtain energy. It has the characteristics of long transmission distance and strong directivity, but it needs to constantly guide the direction of the microwave [13], and will cause harmful effects on the organism, so the application scenario is limited. When transmitting at a short distance (several millimeters to several centimeters), the efficiency can reach 70%-80%. However, when the distance is more than 5 centimeters, the efficiency can be reduced to less than 50%. By virtue of the energy storage field characteristics of non-radiating electromagnetic near-field and the principle of photon tunnel effect, magnetic resonance coupling "captures" the evanescent waves emitted by high-frequency power sources through resonance, thus achieving wireless transmission of electric energy [14]. It has the characteristics of large transmission power, high transmission efficiency and far transmission efficiency. When the transmission distance is within tens of centimeters, the efficiency can be stabilized at about 80%, and it is harmless to human body, making it the most popular development direction in radio energy

transmission technology [15]. Based on the above characteristics, this paper adopts the magnetic resonance coupling WPT technology, which has no harm to human body, high efficiency and greater transmission power, as the power transmission mode.

### 2.2 WPT Circuit Topology Analysis

The WPT (Wireless Power Transfer) circuit topology can be divided into four basic ones based on the differences in the compensation structures of the transmitting and receiving ends: series-series (SS), series-parallel (SP), parallel-series (PS), and parallel-parallel (PP) [16]. Other topologies are developed from these.

The SS-type is easy to understand and implement with stable output characteristics, but has low transmission efficiency. The SP-type has high transmission efficiency and strong adaptability to load changes, yet its resonant compensation capacitor varies with load resistance and needs dynamic adjustment according to the load, making it difficult to implement. The PS-type is similar to the SP-type, both having high transmission efficiency and complex dynamic adjustment and compensation. The PP-type has high transmission efficiency and certain adaptability, but its components need to withstand high voltages, so it has high requirements for components.

In conclusion, the SS-type has stable output characteristics, simple adjustment strategy when the load changes, and lower cost compared to others. Thus, it has broader applicability and research value in the WPT field.

However, the SS compensation structure has the defect of poor transmission efficiency and does not have strong anti-drift ability of coupling coil. In view of this, many studies have focused on improving its structure. In the process of improvement, the SS compensation structure has the characteristics of low cost and convenient dynamic adjustment, and is committed to improving its transmission efficiency and enhancing the output stability, so as to achieve performance optimization and improvement, so that it can better meet the needs of practical applications [17].

In view of the low transmission efficiency and insufficient anti-migration capability of SS compensation topology, DLCC compensation network structure emerged as an improved topology based on SS type. This structure forms a more complex resonant network by adding additional inductors and capacitors at the sending end [18]. This topology provides multiple resonant frequency points, and to a certain extent is less sensitive to changes in load and coupling coefficient, and can effectively transfer more power to the secondary side when the coil is offset, significantly improving the stability of the system transmission. DLCC not only inherits the advantages of SS type, such as low cost and easy dynamic adjustment, but also realizes the decoupling of system resonance frequency from coil coupling coefficient and load, and has the ability of constant current output, so it has become a hot topology structure in current research [19].

Although DLCC compensation network structure has obvious advantages in improving the transmission stability of the system, it has not been widely used. This is mainly because its structural characteristics determine the need to use a large and small coupling coil structure at the sending end and the receiving end, and a single size coil cannot be used only at one end. And in the high-power transmission scenario, a larger flat coil must be used, and the charging gun as a very suitable scenario for the application of WPT technology, because of its narrow and slender internal space, this large flat coil cannot be used at all. Therefore, the DLCC compensation network structure can only stay at the theoretical level, and it is difficult to promote and apply on a large scale in practice, which also limits further expansion of this technology in the field of electric vehicle charging to a large extent.

### 2.3 Analysis of the Influence of Coil Offset on Radio Energy Transmission

At present, ABB's new Terra HP charging pile offers a high-power 350 kW charge. Unstable charging at this level can disrupt the grid and harm batteries. For the grid, it may cause load fluctuations, voltage instability, and harmonic interference. This impacts the overall grid stability and other equipment. For batteries, unstable power can lead to overcharging or undercharging, reducing lifespan and increasing failure risks like overheating or fire, jeopardizing electric vehicle safety and performance. Therefore, studying the fluctuation of transmission power is meaningful for promoting WPT.

In radio energy transmission, stability is affected by factors like coil dislocation, load power fluctuation, electromagnetic interference, and obstacles. The obstacle factor can be mitigated with foreign body detection. Electromagnetic interference is negligible due to its minor impact. Electric vehicles, being slow and predictable in their charging process, have limited effects on the grid and batteries. Based on the above situation, this paper will focus on coil dislocation, exploring its influence mechanism and characteristics on radio energy transmission.

During the actual operation of the charging gun, the coupling coil may be mislocated due to factors such as insertion link, vibration and human operation [20]. Specifically, when the charging gun is inserted, if it is not accurately aligned and fixed, or when the vehicle is charged and swayed by the behavior of people getting on and off the vehicle, or because of artificial careless touch during charging, the position of the coil may be offset.

Coil misalignment can be divided into two categories: distance misalignment and angle misalignment. According to the analysis of the two cases [21], with the gradual increase of the dislocation distance, the transmission efficiency will first show a downward trend and then rise until it finally approaches zero. Correspondingly, the output power will first increase when the dislocation distance increases and then gradually decrease. However, whether it is transmission efficiency or output power, it produces relatively small changes in the face of angular offset.

In view of this, this paper will focus on how to effectively reduce the impact of distance dislocation on output efficiency to carry out in-depth research.

### 2.4 Latest Progress in Efficiency Optimization

SS topology of the planar spiral coil is used to conduct

research, and the results show that within the range of 0 to 15 cm, the maximum transmission efficiency between the sending coil and the receiving coil can only reach 90%, and the efficiency will fluctuate greatly with the change in the distance between them, and the fluctuation range can reach 5% [22].

Anti-offset experiments were carried out using the planar helical coil DLCC compensation circuit, and an output power of 3.4 kW was obtained in an air gap of 150mm, with a DC-DC efficiency of 95.5%. With a gap of 150mm, the transmission power is twice that of a single-coupled WPT system with only main-coil coupling [23]. Moreover, when the distance between the sending coil and the receiving coil is within 0-15cm, the efficiency changes by only 2%. Through comparison, it can be seen that the DLCC topology is superior to the SS topology in terms of transmission efficiency and stability, which is consistent with the previous analysis.

Exploring circuit topology reveals that its characteristics and limitations are significantly influenced by the coupling coil. Space constraints make spiral-coupled coils suitable for charging guns, but their three-dimensional magnetic fields are complex, making direct analysis difficult. Spiral coupling coils can be approximated as planar ones for further study. Comparison of circular and square coils under offset conditions shows circular coils maintain about 70% transmission efficiency with a 10 cm lateral offset and higher output power than square coils. Optimizing circular coil parameters and adding an E-type ferrite core can achieve 85% efficiency at a 20 cm offset. Thus, this paper applies a spiral circular coupling coil with a magnetic core to the WPT coupling coil of the charging gun for related research [24].

### 2.5 Purpose

This paper aims to advance the use of radio energy transmission for electric vehicle charging by innovatively integrating this technology with charging guns. To address the issue of coupling coil displacement, which can increase grid load and reduce battery life, we propose a new structure using magnetic resonance coupling. We also introduce an enhanced DLCC compensation circuit with a spiral insert circular coupling coil and magnetic core, improving and stabilizing transmission efficiency. The sending and receiving coils are of the same size, making them ideal for charging gun applications.

In this paper, the topology structure of the double-coupled LCC circuit is derived in detail. Then, using ANSYS finite element analysis software, a simulation model is made for the placement of magnetic cores in different positions of the spiral insert coupling coil. Finally, in order to quantify the anti-migration performance of the coupling mechanism, the proposed structure is modeled, verified and optimized by Matlab to enhance its output stability. The simulation results show that by using the new two-sided LCC compensation circuit structure proposed in this paper and placing the magnetic core outside the helical plug-in coupling coil, the transmission efficiency offset can be effectively controlled within 0.4% when the coil offset ranges from 0 to 30mm, which verifies the effectiveness of the design scheme in the study of anti-offset.

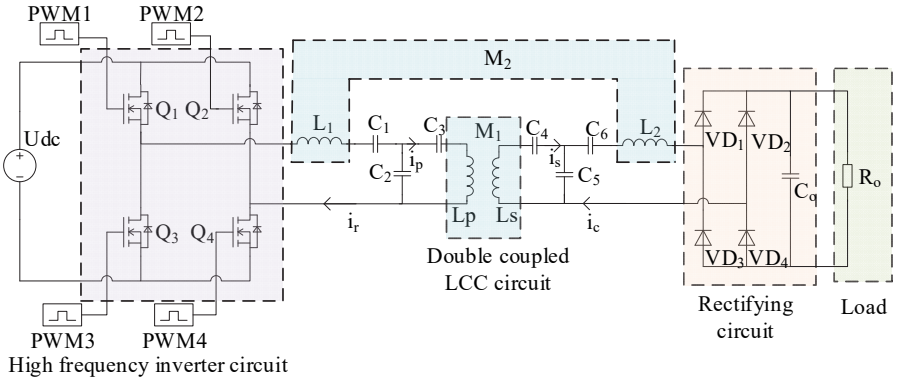


**Figure 1** Dual coupling LCC circuit topology

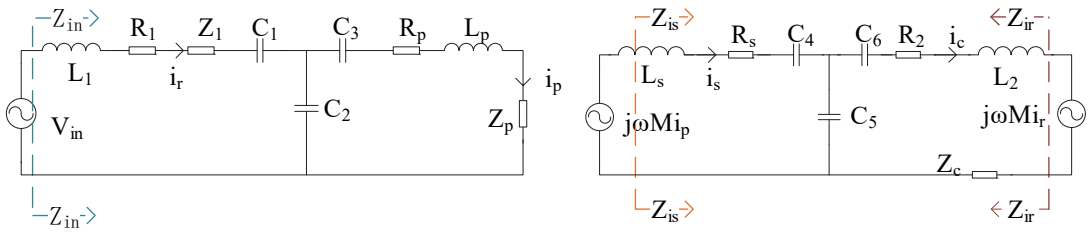


a) Transmitting circuit b) Receiving circuit

**Figure 2** Equivalent circuit

## 3 RESEARCH METHODOLOGY

### 3.1 Circuit Topology

The circuit topology of the double-coupled LCCWPT system is shown in Fig. 1. The inductors $L_p$ and $L_s$ constitute the main coupler, and the mutual inductance value is defined as $M_1$. Inductors $L_1$ and $L_2$ constitute the main coupler, whose mutual inductance value is defined as $M_2$.

The circuit topology can be divided into the sending

end and the receiving end. The sending end: $U_{dc}$ is the DC power supply, and the switching tube $Q_1$~$Q_4$ is the high-frequency inverter circuit. $i_r$/$i_p$, and $i_c$ are the currents on $L_1$, $L_p$, $L_2$ and $L_s$, respectively. The primary side $L_1$ and $C_1$, $C_2$ constitute the resonator, and $L_p$, and $C_2$, $C_3$ constitute the resonator. The secondary $L_s$ and $C_4$, $C_5$ form a resonator, $L_2$ and capacitors $C_5$ and $C_6$ form a resonator. When the charging gun input and output are only using the same size coupling coil, it can meet the practical use needs, so $L_1 = L_p$, $L_2 = L_s$, which leads to the conclusion $C_1 = C_2 = C_3$, $C_4 = C_5 = C_6$. Output terminal: $VD_1$~$VD_4$ constitutes a rectifier circuit; $C_o$ is the filter capacitor, $R_o$ is the load resistance.

### 3.2 Principle Analysis

Considering the energy transmission characteristics of the coupling coil, the magnetic resonance coupling circuit can be simplified by using the mutual inductance equivalent model, as shown in Fig. 2. $V_{in}$ is the square wave voltage output by the inverter, which can be regarded as sine wave after LC filtering. When the circuit is running, the current will generate induced electromotive force $j\omega Mi_r$ and $j\omega Mi_p$ respectively on the secondary side after passing through the sending coils $L_1$ and $L_p$. $R_1$, $R_p$, $R_s$ and $R_2$ are the equivalent internal resistance of the primary side coil $L_1$ and $L_p$ and the secondary side coil $L_s$ and $L_2$, respectively. When the secondary side coil is coupled with the primary side coil, a reflection impedance is generated in the primary side coil. $Z_1$ and $Z_p$ are the reflected impedance of the primary side coil $L_1$ and $L_p$ respectively, and $Z_c$ is the output impedance.

$L_1$ resonates with $C_1$ and $C_2$ on the primary side, and $L_p$ resonates with $C_2$ and $C_3$. The secondary $L_s$ resonates with $C_4$ and $C_5$, and $L_2$ resonates with $C_5$ and $C_6$. The transmitters $L_1$ and $L_p$ use the same coupling coil, $C_1 = C_2 = C_3$, so $R_1 = R_p$. The receivers $L_s$ and $L_2$ use the same coupling coil, $C_4 = C_5 = C_6$, so $R_2 = R_s$.

Due to the resonant cavity acting as a low-pass filter during circuit operation, high-order harmonic currents can be ignored. Further analyze the working principle of the circuit using the superposition theorem, considering the effects of couplers $L_1$-$L_2$ and $L_p$-$L_s$ respectively, as shown in Figs. 3 and 4.

To simplify the analysis, use the zero point of the $C_2$ voltage as the boundary. When the voltage of $C_2$ is greater than zero, the transmitting terminals $L_1$, $C_1$ and $C_2$ form a resonant cavity circuit with a resonant angular frequency of $\omega_1 = 1/\sqrt{L_1C_1C_2/(C_1+C_2)}$, the receiver $L_2$, $C_5$ and $C_6$ form a resonator, and the resonant angular frequency is $\omega_4 = 1/\sqrt{L_2C_5C_6/(C_5+C_6)}$. Due to the impedance of the parallel resonant circuit approaching infinity, it can be considered that $L_p$ and $L_s$ are open circuits.

When $C_2$ voltage is greater than zero, the sending end $L_p$, $C_2$, $C_3$ form the resonator circuit, the resonant angular frequency is $\omega_2 = 1/\sqrt{L_pC_2C_3/(C_2+C_3)}$, the receiving end $L_s$, $C_4$, $C_5$ form the resonator cavity, the resonant angular frequency is $\omega_3 = 1/\sqrt{L_SC_4C_5/(C_4+C_5)}$ Since the impedance of the parallel resonant circuit is close to infinity, $L_p$ and $L_2$ can be considered open circuit.

By analyzing the responses generated by $L_1$ and $L_p$ in the secondary side circuit separately, and then superimposing their effects, the overall response of the secondary side receiving circuit can be obtained [25]. This method helps to better understand and analyze the roles of various power sources in complex circuits and their impact on the entire circuit.

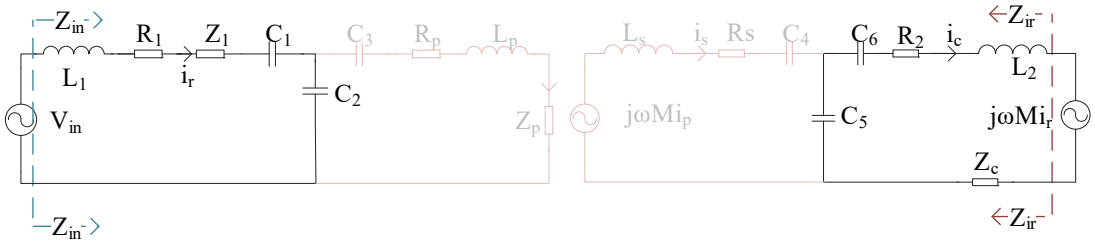


a) Transmitting circuit b) Receiving circuit

**Figure 3** Power driven resonant circuit

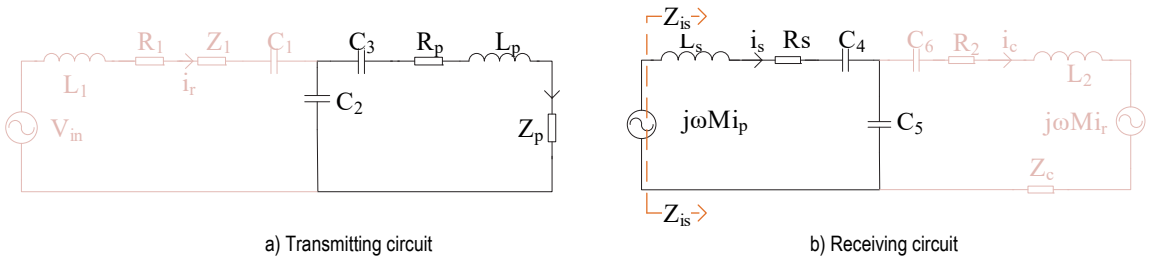


a) Transmitting circuit b) Receiving circuit

**Figure 4** Independent resonant circuit

### 3.3 System Efficiency Analysis

The overall impedance of the LCC compensation topology from its input end is $Z_{in}$. Using Kirchhoff's voltage law to analyze the circuit, the impedance expression can be obtained as:

$$Z_{in} = \left(j\omega L_1 + Z_1 + R_1 + \frac{1}{j\omega C_1}\right) // \left(j\omega L_P + \frac{1}{j\omega C_3} + R_P + Z_P\right) // \frac{1}{j\omega C_2} \quad (1)$$

The overall impedance of the LCC compensation topology on the secondary side when viewed from $L_S$ is $Z_{is}$, and its impedance expression is:

$$Z_{is}=\left(j\omega L_S+R_S+\frac{1}{j\omega C_4}\right)//\left(j\omega L_2+R_4+Z_C+\frac{1}{j\omega C_6}\right)//\frac{1}{j\omega C_5} \tag{2}$$

The overall impedance of the LCC compensation topology on the secondary side when viewed from $L_2$ is $Z_{ir}$, and its impedance expression is:

$$Z_{ir}=\left(j\omega L_2+R_2+Z_C+\frac{1}{j\omega C_6}\right)//\left(\frac{1}{j\omega C_4}+j\omega L_S+R_S\right)//\frac{1}{j\omega C_5} \tag{3}$$

When both the primary and secondary sides of the system are in a resonant state, the resonant frequency is equal to the operating frequency, the input impedance is purely resistive, and the same type of coupling coil is used for both the transmitting and receiving ends [26]. So, Eqs. (1), (2), and (3) can be simplified to obtain:

$$Z_{in}^{'}\approx R_1+Z_1 \tag{4}$$

$$Z_{is}^{'}\approx R_s \tag{5}$$

$$Z_{ir}^{'}\approx R_4+Z_C \tag{6}$$

The expressions for reflected impedance $Z_1$ and $Z_P$ are as follows:

$$Z_1=\frac{\omega^2M^2}{R_4+Z_C} \tag{7}$$

$$Z_P=\frac{\omega^2M^2}{R_s} \tag{8}$$

Further derive output efficiency $\eta$:

$$\eta=P_o/P_i=\frac{\omega MZ_c\left(R_s+R_4+Z_c\right)^2\cdot\left(R_4+Z_c\right)}{Z_c\cdot R_s\left(R_4+Z_c\right)^2\cdot\left(\omega M^2+R_1\right)} \tag{9}$$

By analyzing Eq. (9), it can be found that mutual inductance, resonant frequency, coil internal resistance, and output load are the main factors affecting output efficiency. In the case of fixed circuit parameters, the output efficiency is mainly affected by the mutual inductance value, and there is a proportional relationship between the output efficiency and the mutual inductance value.

### 3.4 WPT without Magnetic Core Simulation

The coupling of two spiral coils can be simplified and analyzed as the coupling of two planar circles [27], as shown in Fig. 4. Taking the coupling between the primary coil $L_p$ and the secondary coil $L_s$ as an example, there is a current $i_p$ flowing through the primary circuit $l_1$, and a current $i_s$ flowing through the secondary circuit $l_2$. After the primary circuit $l_1$ is powered on, a magnetic flux $l_2$ will be generated on the secondary circuit $\psi$.

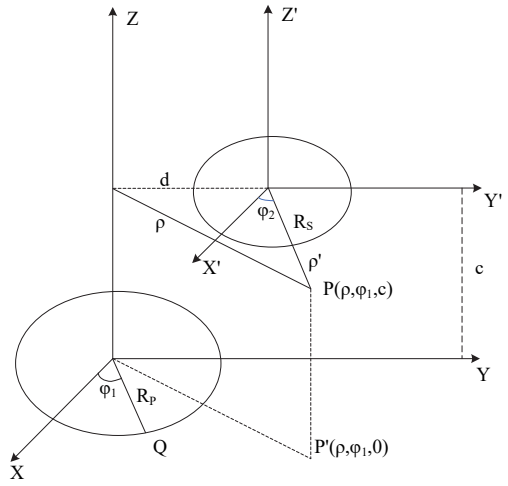


**Figure 5** Lateral offset with parallel axis and two circular coil structures

According to the Newman integral formula, the mutual inductance between any two closed coils can be calculated as follows:

$$M=\frac{\mu_0}{4\pi}\int_0^{2\pi}\int_0^{2\pi}\frac{R_{r1}R_{r2}\cos(\varphi_1-\varphi_2)d\varphi_1d\varphi_2}{R} \tag{10}$$

Eq. (10) is the Newman integral formula, where $\mu_0=4\pi\cdot10^{-7}\mathrm{H/m}$ is the magnetic permeability in vacuum; $R$ is the distance between source point $Q$ and field point $P$; $R_{r1}$ and $R_{r2}$ are the radii of the main coil and sub coil, respectively; $D$ is the distance between the two coil axes; $C$ is the distance between the planes where the two coils are located [28]. When the coil radius parameter is determined, the mutual inductance between the two coils is inversely correlated with the distance, and as the distance increases, the mutual inductance decreases [29].

In Maxwell electromagnetic simulations, we construct the environment using a global coordinate system. Areas without specified materials are filled with air to mimic real-world conditions. Boundary conditions are set with a 20% offset in the $X$ and $Y$ directions and a 1000% offset in the $Z$ direction to accommodate limited internal space within the charging gun. This setup ensures accurate simulation and analysis of coupling coil characteristics and changes.

When the number of turns of the coupling coil is fixed, the smaller the coil interval is, the higher the transmission efficiency will be [30]. Due to the limitations of the coil processing process, an interval of 1 mm is already a relatively small distance for the coils to be close to each other. In addition, when designing the coupling coil, the internal space and heat dissipation requirements of the charging gun must be taken into consideration because the

greater the power is, the more heat will be generated by the coupling coil. Therefore, the use of a multi-coupling coil structure with a small size can greatly reduce the difficulty of heat dissipation.

At the same time, considering that the actual charging pile generally uses high-frequency power supplies, in this case, the diameter of the coupling coil should be reduced as much as possible on the basis of ensuring that it can carry a certain current. The specific parameters of the transmitting coil and the receiving coil for radio energy transmission are shown in Tab. 1.

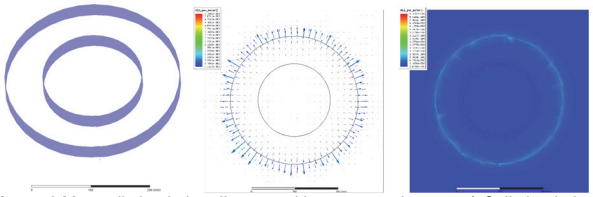

**Figure 6** Maxwell simulation diagram without magnetic core: a) Coil simulation; b) Magnetic field distribution cloud; c) Magnetic field vector

**Table 1** Parameter values of magnetic resonance coupled wireless charging system

| | Turns | Wire diameter / cm | Diameter / mm | Turn spacing / mm | Material |
|---|---|---|---|---|---|
| Large size coil $W_1$ | 30 | 0.5 | 85 | 1 | Copper |
| Small size coil $W_2$ | 30 | 0.5 | 150 | 1 | copper |

The transmitting coil uses large-sized coils $W_1$, and the receiving coil uses small-sized coils $W_2$. The transmitting coil and the receiving coil are arranged in concentric circles on the same plane. Simulate the coil using Maxwell, and the simulated coil structure is shown in Fig. 6a. The magnetic field distribution cloud map is shown in Fig. 6b. The magnetic field vector diagram is shown in Fig. 6c.

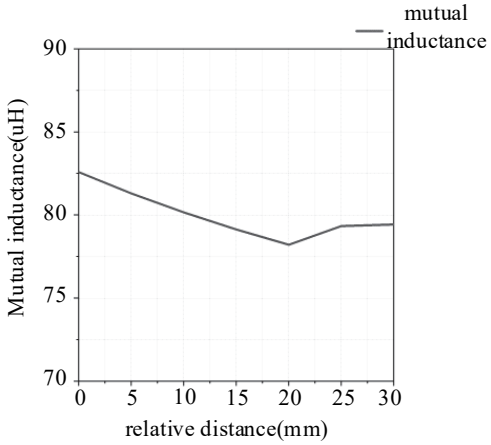


**Figure 7** The variation curve of mutual inductance value with coil offset under the condition of no magnetic core

Due to the limited space inside the charging gun, the mismatch distance of the coupling coil has more influence on the performance than the offset Angle in practice. In addition, compared with the offset Angle, the dislocation distance of the coupling coil has a more prominent influence on its performance [31]. Therefore, in this study, the misalignment distance of coupling coils is set to vary within the range of 0~30 mm. On the premise of keeping the position of $W_1$ fixed, make $W_2$ move horizontally with a step length of 5 mm, starting from the relative distance of 0 mm between them, and gradually moving to the position of 30 mm. In this process, the change data of mutual inductance value is recorded in detail, and the result is shown in Fig. 7.

As shown in Fig. 7, the mutual inductance value reaches its peak when the relative distance between the receiving coil and the transmitting coil is 0 mm, which is consistent with the analysis in the previous text. Although the mutual inductance value has a smaller impact on the relative distance between the two coils compared to a planar spiral coil, there is still room for optimization. This is because in the practical application scenario, Eq. (9) shows that even if the change of mutual inductance value is relatively small, such subtle changes will directly affect the transmission efficiency, grid fluctuations and short battery life under the cumulative effect.

### 3.5 WPT with Magnetic Core Simulation

The high permeability of the magnetic core allows system optimization by adding a core that constrains the magnetic field direction, increases inductance, reduces leakage, and enhances effective field lines. Tab. 2 lists common cores; MPP is chosen for its high conductivity and moderate flux density, minimizing eddy current loss in high-frequency applications. The relatively small eddy current loss is often negligible in actual scenarios, not significantly impacting overall performance.

It is worth mentioning that Maxwell software is pre-set with a variety of magnetic core parameters. When using the software, you only need to select the corresponding magnetic core in the software according to actual requirements, and Maxwell can accurately calculate the mutual inductance according to the characteristics of the selected magnetic core material. This provides great convenience and strong technical support for our research and analysis.

**Table 2** Common core types and electromagnetic parameters

| | Conductivity $\sigma$ / S/m | Relative permeability / μr | Relative permeability / μr | Applicable frequency |
|---|---|---|---|---|
| Manganese zinc ferrite | $1 \times 10^{-6}$ | 2000 | 0.3~0.5 | 1~500 kHz |
| Molybdenum Permo alloy powder core | $1 \times 10^{6}$ | 550 | 0.7 | Below 300 kHz |
| Silicon steel sheet | 6.666666 | 7000 | 1.5~2 | 50~400 Hz |
| Ferrosialum | $9.3 \times 10^{6}$ | 60 | 1 | Max. 20 MHz |

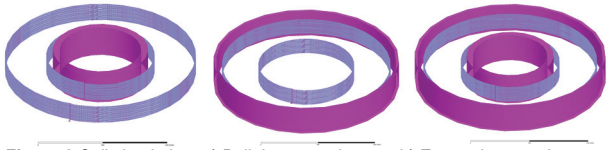

**Figure 8** Coil simulation: a) Built in magnetic core; b) External magnetic core; c) Dual magnetic core

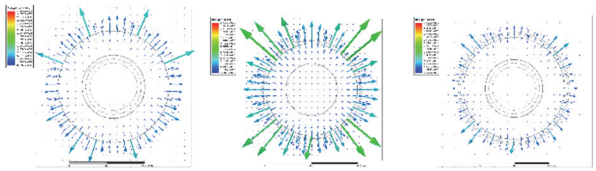

**Figure 9** Magnetic field distribution cloud: a) Built in magnetic core; b) External magnetic core; c) Dual magnetic core

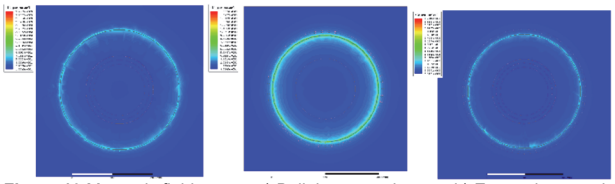

**Figure 10** Magnetic field vector: a) Built in magnetic core; b) External magnetic core; c) Dual magnetic core

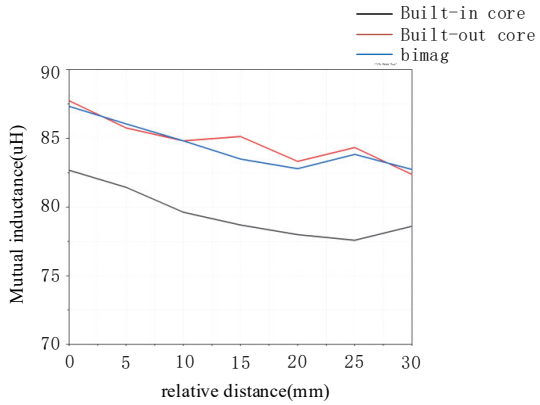


**Figure 11** Curve graph of mutual inductance value changing with offset

**Table 3** Magnetic core parameters

| | Inner diameter of magnetic core /mm | Outer diameter of magnetic core /mm | Length of magnetic core /mm | Magnetic core material |
|---|---|---|---|---|
| Inner magnetic core of receiving coil | 65 | 75 | 50 | MPP |
| Send the outer magnetic core of the coil | 155 | 165 | 50 | MPP |

By observing the chart, it can be seen that after adding the magnetic core, the mutual inductance value reaches its maximum when the relative distance between the coupled coils is zero, consistent with the analysis above. When the coupling coil has an external magnetic core and a dual magnetic core, the mutual inductance value shows a large value, but it is impossible to determine which structure can make the output efficiency the most stable solely based on the mutual inductance value.

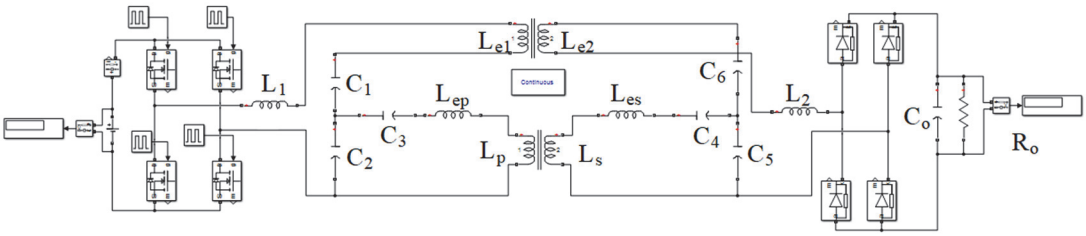


**Figure 12** Circuit simulation diagram

This is because after adding a magnetic core, the inductance value of the coil is not fixed, but changes with the magnetic permeability and placement of the core [32]. The analysis process of calculating output efficiency through mutual inductance is quite complex. So, this article uses Matlab to analyze which structure is more conducive to outputting stable power.

## 4 RESULTS AND DISCUSSION

Based on the double-coupled LCC topology studied above, the model is built in Matlab to carry out simulation analysis of the transmission coil structure. When selecting the magnetic core mentioned above, a low eddy current loss has been selected, so when introducing the magnetic core, only the mutual inductance value needs to be brought into Matlab, and the circuit simulation diagram is shown in Fig. 12. $L_1$ and $L_p$ use large-sized coils $W_1$, while $L_2$ and $L_s$ use small-sized coils $W_2$. $L_{e1}$, $L_{ep}$, $L_{e2}$, and $L_{es}$ represent the leakage inductance of $L_1$, $L_p$, $L_2$ and $L_s$, respectively. It can be seen from Eq. (10) that when the distance between the coupling coils is closest, the mutual inductance value is the largest, and it can be seen from equation 9 that the mutual inductance value will directly affect the transmission efficiency. Therefore, in order to reduce the fluctuation of transmission efficiency, the circuit parameters are calculated when the coil distance is 30 mm. Other circuit parameters are shown in Tab. 4. Combining the above parameters with the simulation results of Maxwell placing magnetic cores at different positions, and inputting them into the model established in Matlab for simulation analysis, the circuit simulation results are shown in Fig. 13.

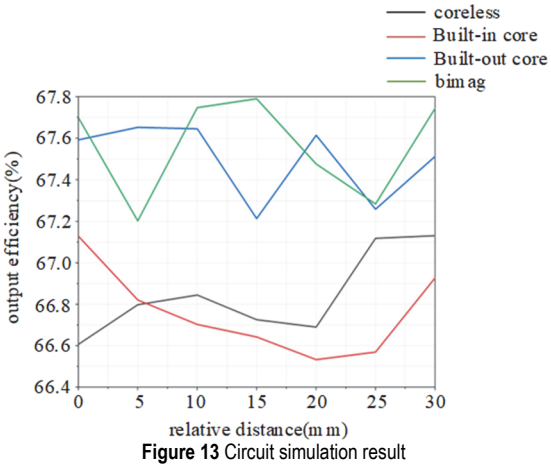


**Figure 13** Circuit simulation result

Under 50 V input, the transmission efficiency fluctuation from 0 mm to 30 mm for different coupling coil structures and different coil displacements is shown in Fig. 13. It can be seen from the simulation results that for the structures with built-in magnetic core and without magnetic core, the transmission efficiency is relatively low and the fluctuation of the transmission efficiency is significant, with the fluctuation of both reaching 0.6%. After the addition of magnetic core, the transmission efficiency of both the external coil structure and the dual

magnetic core structure is improved. Specifically, the transmission efficiency of the external coil structure is 0.4% and that of the dual magnetic core structure is 0.6%. It is worth noting that these structures can achieve their maximum transmission efficiency at relative distances of 0 mm and 30 mm respectively.

**Table 4** Bilateral LCC type WPT system parameters

| Parameter | Value |
|---|---|
| Input voltage $U_{dc}$ / V | 50 |
| Switching frequency $f$ / kHz | 50 |
| Primary side capacitor $C_1$ / nF | 40 |
| Primary side capacitor $C_2$ / nF | 40 |
| Primary side capacitor $C_3$ / nF | 40 |
| Secondary side capacitor $C_4$ / nF | 80 |
| Secondary side capacitor $C_5$ / nF | 80 |
| Secondary side capacitor $C_6$ / nF | 80 |
| Output capacitance $C_o$ / nF | 100 |
| Equivalent load on output side $R_o$ / Ω | 100 |

With the change of coil offset distance, the transmission power change is only 0.4%, which can greatly improve the anti-offset ability of WPT and the stability of power transmission. However, the internal space of the charging gun is narrow and slender, which is not suitable for the large flat coil. Therefore, DLCC is difficult to promote and apply on a large scale in practice, which also limits further expansion of this technology in the field of electric vehicle charging to a large extent.

## 5 CONCLUSION

Wireless power transmission (WPT) technology for electric vehicles (EVs) holds significant promise for improving charging convenience and efficiency. However, practical challenges, such as coil misalignment, lead to fluctuations in power transmission efficiency.

In this paper, a double-coupled LCC compensation circuit with helical coupling coil with external magnetic core is used to improve the anti-migration ability of WPT, and enhance the transmission efficiency and stability of WPT. The simulation model is established by ANSYS, and the performance is verified by MATLAB. In the displacement range from 0 to 30 mm, the transmission efficiency deviation of the proposed structure can be controlled within 0.4%. These results prove that the proposed method is effective in improving the WPT reliability of EV applications, and provides a promising solution for its application in real-world scenarios. The following conclusions are drawn:

1) The insertion type spiral coil structure, with the addition of a magnetic core on the outer side of the transmitting coil, not only enhances self-inductance while effectively reducing magnetic leakage, but also significantly improves the mutual inductance between the coils.

2) After adding a magnetic core on the outer side of the transmitting coil, the insertion type spiral coil structure can stabilize the output efficiency by effectively constraining the magnetic field lines even if the small-sized coupling coil is displaced, thereby greatly improving the anti-interference ability and stability of the system.

3) By using the novel bilateral LCC compensation circuit structure proposed in this article and placing a magnetic core outside the spiral insertion coupling coil, the offset of output efficiency can be effectively controlled within 0.4% when the coil is offset within the range of 0-30 mm.

However, at present, it only stays in the simulation stage. In the future, real machine verification can be carried out on the basis of this research, and how to further improve the transmission efficiency can be discussed.

**Acknowledgements:**

The paper was funded by the Key Project of the Research Fund of North China Institute of Aerospace Engineering (P. No. ZD202206) and Central Guidance for Local Science and Technology Development Fund Project (Free Exploration Basic Research) (P. No. 246Z4418G).

## 6 REFERENCES

[1] Brown, W. C. (1996). The history of wireless power transmission. *Solar energy*, *56*(1), 3-21. https://doi.org/10.1016/0038-092X(95)00080-B

[2] Jia, Z., Yan, G., Liu, H., Wang, Z., Jiang, P., & Shi, Y. (2012). The optimization of wireless power transmission: design and realization. *The International Journal of Medical Robotics and Computer Assisted Surgery*, *8*(3), 337-347. https://doi.org/ 10.1002/rcs.1428

[3] Garnica, J., Chinga, R. A., & Lin, J. (2013). Wireless power transmission: From far field to near field. *Proceedings of the IEEE*, *101*(6), 1321-1331. https://doi.org/10.1109/JPROC.2013.2251411

[4] McSpadden, J. O. & Mankins, J. C. (2002). Space solar power programs and microwave wireless power transmission technology. *IEEE microwave magazine*, *3*(4), 46-57. https://doi.org/10.1109/MMW.2002.1145675

[5] Bukya, R., Madhu Mohan, G., & Kumar Swamy, M. (2024). Artificial intelligence role in optimizing electric vehicle charging patterns, reduce costs, and improve overall efficiency: A review. *Journal of Engineering, Management and Information Technology*, *2*(3), 129-138. https://doi.org/10.61552/JEMIT.2024.03.004

[6] Zhang, L., Tian, Z., Li, Z., Cheng, S., Wang, Y., Eldeeb, H. H., & Zhao, H. (2023). Parallel contactless transmission of power and rotor temperature of electrical machines via magnetically-coupled resonance and capacitive radio frequency. *IEEE Transactions on Industry Applications*, *59*(4), 3955-3965. https://doi.org/10.1109/TIA.2023.3262628

[7] Collado, A. & Georgiadis, A. (2014). Optimal waveforms for efficient wireless power transmission. *IEEE microwave and wireless components letters*, *24*(5), 354-356. https://doi.org/10.1109/LMWC.2014.2309074

[8] Boussaada, M., Abdelati, R., Lahdhiri, H., & Yahia, H. (2023). PV characterization and MPPT based on characteristic impedance using Arduino board and MATLAB interface. *Studies in Informatics and Control*, *32*(1), 91-100. https://doi.org/10.24846/v32i1y202309

[9] Buja, G., Bertoluzzo, M., & Mude, K. N. (2015). Design and experimentation of WPT charger for electric city car. *IEEE Transactions on Industrial Electronics*, *62*(12), 7436-7447. https://doi.org/10.1109/TIE.2015.2455524

[10] Zakerian, A., Vaez-Zadeh, S., & Babaki, A. (2019). A dynamic WPT system with high efficiency and high power factor for electric vehicles. *IEEE Transactions on Power Electronics*, *35*(7), 6732-6740. https://doi.org/10.1109/TPEL.2019.2957294

[11] Shinohara, N. (2012). The wireless power transmission: inductive coupling, radio wave, and resonance coupling. *Wiley Interdisciplinary Reviews: Energy and Environment*, *1*(3), 337-346.

[12] Rituraj, G., Joy, E. R., Kushwaha, B. K., & Kumar, P. (2014, October). Analysis and comparison of series-series and series-parallel topology of contactless power transfer systems. *TENCON 2014-2014 IEEE Region 10 Conference*, 1-6. https://doi.org/10.1109/TENCON.2014.7022440

[13] Ren, J., Hu, J., Zhang, D., Guo, H., Zhang, Y., & Shen, X. (2018). RF energy harvesting and transfer in cognitive radio sensor networks: Opportunities and challenges. *IEEE Communications Magazine*, *56*(1), 104-110. https://doi.org/10.1109/MCOM.2018.1700519

[14] Ping, H., Xiaowei, Z., & Congshan, L. (2023). Smooth Regulation of DC Voltage in VSC-MTDC Systems Based on Optimal Adaptive Droop Control. *Technical gazette*, *30*(4),1234-1240. https://doi.org/10.17559/TV-20220806130349

[15] Schulze, J., Schüngel, E., & Czarnetzki, U. (2009). The electrical asymmetry effect in capacitively coupled radio frequency discharges-measurements of dc self-bias, ion energy and ion flux. *Journal of Physics D: Applied Physics*, *42*(9), 092005. https://doi.org/10.1088/0022-3727/42/9/092005

[16] Shinohara, N. (2020). Trends in wireless power transfer: WPT technology for energy harvesting, mllimeter-wave/THz rectennas, MIMO-WPT, and advances in near-field WPT applications. *IEEE microwave magazine*, *22*(1), 46-59. https://doi.org/10.1109/MMM.2020.3027935

[17] Zhao, H., Wang, Z., Wang, Y., Zhang, L., Eldeeb, H. H., Zhan, Y., & Xu, G. (2021, October). Electromechanical based energy saving control strategy for beam pumping motor systems in oil production industry. *2021 IEEE Industry Applications Society Annual Meeting (IAS)*, 1-8. https://doi.org/10.1109/IAS48185.2021.9677220

[18] Kim, D., Abu-Siada, A., & Sutinjo, A. (2018). State-of-the-art literature review of WPT: Current limitations and solutions on IPT. *Electric Power Systems Research*, *154*, 493-502. https://doi.org/10.1016/j.epsr.2017.09.018

[19] Kim, S. H., Park, T. S., Yoo, J. Y., & Park, G. T. (2001). Speed-sensorless vector control of an induction motor using neural network speed estimation. *IEEE Transactions on industrial electronics*, *48*(3), 609-614. https://doi.org/10.1109/41.925588

[20] Hahn, S., Kim, Y., Ling, J., Voccio, J., Park, D. K., Bascuñán, J., & Iwasa, Y. (2013). No-insulation coil under time-varying condition: Magnetic coupling with externalcoil. *IEEE transactions on applied superconductivity*, *23*(3), 4601705-4601705. https://doi.org/10.1109/TASC.2013.2240756

[21] Huang, C. Y., James, J. E., & Covic, G. A. (2014). Design considerations for variable coupling lumped coil systems. *IEEE transactions on Power Electronics*, *30*(2), 680-689. https://doi.org/10.1109/TPEL.2014.2311818

[22] Cannon, B. L., Hoburg, J. F., Stancil, D. D., & Goldstein, S. C. (2009). Magnetic resonant coupling as a potential means for wireless power transfer to multiple small receivers. *IEEE transactions on power electronics*, *24*(7), 1819-1825. https://doi.org/10.1109/TPEL.2009.2017195

[23] Zierhofer, C. M. & Hochmair, E. S. (1996). Geometric approach for coupling enhancement of magnetically coupled coils. *IEEE transactions on Biomedical Engineering*, *43*(7), 708-714. https://doi.org/10.1109/TPEL.2009.2017195

[24] Han, C., Harrold, T., Armour, S., Krikidis, I., Videv, S., Grant, P. M., ... & Hanzo, L. (2011). Green radio: radio techniques to enable energy-efficient wireless networks. *IEEE communications magazine*, *49*(6), 46-54. https://doi.org/10.1109/MCOM.2011.5783984

[25] Lee, S., Zhang, R., & Huang, K. (2013). Opportunistic wireless energy harvesting in cognitive radio networks. *IEEE Transactions on Wireless Communications*, *12*(9), 4788-4799. https://doi.org/10.1109/TWC.2013.072613.130323

[26] Banciu, D., Vevera, A. V., & Popa, I. (2023). Digital transformation impact on organization management and several necessary protective actions. *Studies in Informatics and Control*, *32*(1),49-56. https://doi.org/10.24846/v32i1y202305

[27] Thirukrishna, J. T., Karthik, S., & Arunachalam, V. P. (2018). Revamp energy efficiency in homogeneous wireless sensor networks using optimized radio energy algorithm (OREA) and power-aware distance source routing protocol. *Future Generation Computer Systems*, *81*, 331-339. https://doi.org/10.1016/j.future.2017.11.042

[28] Yin, S., Wang, L., Wang, Q., Ivanović, M., & Yang, J. (2023). M2F2-RCNN: Multi-functional Faster RCNN Based on Multi-scale Feature Fusion for Region Search in Remote Sensing Images. *Computer Science and Information Systems*, *20*(4). https://doi.org/10.2298/CSIS230315054Y

[29] Wang, S., Song, A., & Qian, Y. (2023). Predicting Smart Cities' Electricity Demands Using K-Means Clustering Algorithm in Smart Grid. *Computer Science and Information Systems*, *20*(2), 657-678. https://doi.org/10.2298/CSIS220807013W

[30] Aka, A. C., Atta, A. F., Keupondjo, S. G. A., & Oumtanaga, S. (2023). An Efficient Anchor-Free Localization Algorithm for all ClusterTopologies in a Wireless Sensor Network. *International Journal of Computers Communications & Control*, *18*(3), 4961. https://doi.org/10.15837/ijccc.2023.3.4961

[31] Bin Y., Huilai L., Ying X., Fuping Z., Chengdong Q., Youzhi S., & Iongbo, W. (2023). Directed Search Based on Improved Whale Optimization Algorithm for Test Case Prioritization. *International Journal of Computers Communications & Control*, *18*(2). https://doi.org/10.15837/ijccc.2023.2.5049

[32] Huang, R. & Zhang, B. (2014). Frequency, impedance characteristics and HF converters of two-coil and four-coil wireless power transfer. *IEEE Journal of Emerging and selected topics in Power Electronics*, *3*(1), 177-183. https://doi.org/10.1109/JESTPE.2014.2315997

**Contact information:**

**Zhen ZHAO**, Associate Professor
North China Institute of Aerospace Industry,
133 Aimin East Road, Langfang, Hebei 065000, P.R. China
E-mail: 15952962@qq.com

**ZeJun ZHAO**, Postgraduate
North China Institute of Aerospace Industry,
133 Aimin East Road, Langfang, Hebei 065000, P.R. China
E-mail: 892729935@qq.com

**XinMiao TENG**, Senior Engineer
CNPC Engineering Technology R&D Company Limited,
Building 1, Courtyard 5, Huanghe Street, Changping District, Beijing, China
E-mail: tengxinmiaodr@cnpc.com.cn

**DeZhou YU**, Senior Engineer
CNPC Engineering Technology R&D Company Limited,
Building 1, Courtyard 5, Huanghe Street, Changping District, Beijing, China
E-mail: tengxinmiaodr@cnpc.com.cn

**Shuyao TIAN**, Associate Professor
North China Institute of Aerospace Industry,
133 Aimin East Road, Langfang, Hebei 065000, P.R. China
E-mail: zhangliancheng@nciae.edu.cn

**Xu LIANG**, Undergraduate
Shenyang Aerospace University,
No. 37 Daoyi South Avenue, Shenbei New Area, Shenyang, China
E-mail: 1737058337@qq.com

**Lian Cheng ZHANG**, Professor
(Corresponding author)
North China Institute of Aerospace Industry,
133 Aimin East Road, Langfang, Hebei 065000, P.R. China
E-mail: zhangliancheng@nciae.edu.cn